

Self-Commissioning of Synchronous Reluctance Motor Drives: Magnetic Model Identification with Online Adaptation

*Original*

Self-Commissioning of Synchronous Reluctance Motor Drives: Magnetic Model Identification with Online Adaptation / Varatharajan, Anantaram; Pellegrino, Gianmario; Armando, Eric. - (2020), pp. 5353-5360. (Intervento presentato al convegno 2020 IEEE Energy Conversion Congress and Exposition (ECCE) tenutosi a Detroit, MI, USA, USA nel 11-15 Oct. 2020) [10.1109/ECCE44975.2020.9236307].

*Availability:*

This version is available at: 11583/2850964 since: 2020-11-03T15:56:48Z

*Publisher:*

IEEE

*Published*

DOI:10.1109/ECCE44975.2020.9236307

*Terms of use:*

This article is made available under terms and conditions as specified in the corresponding bibliographic description in the repository

*Publisher copyright*

IEEE postprint/Author's Accepted Manuscript

©2020 IEEE. Personal use of this material is permitted. Permission from IEEE must be obtained for all other uses, in any current or future media, including reprinting/republishing this material for advertising or promotional purposes, creating new collecting works, for resale or lists, or reuse of any copyrighted component of this work in other works.

(Article begins on next page)

# Self-Commissioning of Synchronous Reluctance Motor Drives: Magnetic Model Identification with Online Adaptation

Anantaram Varatharajan  
*Department of Energy*  
*Politecnico di Torino*  
 Turin, Italy

anantaram.varatharajan@polito.it

Gianmario Pellegrino  
*Department of Energy*  
*Politecnico di Torino*  
 Turin, Italy

gianmario.pellegrino@polito.it

Eric Armando  
*Department of Energy*  
*Politecnico di Torino*  
 Turin, Italy

eric.armando@polito.it

**Abstract**—A new magnetic model self-identification technique is proposed to build the flux-map look-up tables (LUTs) for synchronous reluctance (SyR) machines. Provided the shaft is free to turn, an alternating acceleration and deceleration sequence is envisaged for identification without a dedicated experimental rig or additional hardware. Respect to previous works, the stator flux and the stator resistance are adapted online during the run, thus eliminating the need for post-processing and the sensitivity to winding temperature variations during the test. Experimental validation on a 1.1 kW SyR motor test-bench shows promising results.

**Index Terms**—Synchronous reluctance machine, magnetic model identification, cross-saturation, self-commissioning

## I. INTRODUCTION

The popularity of synchronous reluctance (SyR) motors for several variable speed applications can be attributed to their high efficiency, robustness, manufacturing simplicity, competitive cost and continuous torque per volume ratio. For SyR motors, the most complicated parameter to be estimated is often the current-to-flux relationship, also called flux-map, which is non-linear due to both self-axis saturation and cross-coupling. The optimal operation for minimizing stator resistance losses lies on the maximum torque per ampere (MTPA) curve. For speeds beyond rated, the control trajectories in flux-weakening operation and the achievable torque limit according to the maximum torque per volts (MTPV) law are retrieved from the post-processing of the flux-map LUTs, as are the optimal operating points for maximum torquer per ampere (MTPA) law at low and nominal speed. This is common for many control schemes: current vector control in [1] and direct flux vector control in [2]. Therefore, the need for complete flux-map of a SyR machine is recognized.

The standard methods for machine magnetic model identification (MMI) [3], [4] require to test the machine in a dedicated laboratory environment. A constant speed test is reported in [4] where the  $dq$  current plane is systematically explored and mapped with alternating motoring and braking operation. Several automatic procedures without additional auxiliary drive are developed [5]–[8]; an AC signal injection with DC bias is proposed in [5] to build the flux-map from incremental

inductance at standstill condition. Dual hysteresis current controllers for rapid torque reversal at standstill is proposed in [6] where the saturation approximating function is computed with multiple linear regression. An alternating acceleration and deceleration test at free-shaft to identify the magnetic model is proposed in [7]. Sensorless self-commissioning techniques to retrieve flux-map of SyR motors are reported in [9]–[13]. A comprehensive review on the commissioning techniques is presented in [14].

Akin to [7], the proposed scheme involves self-acceleration and deceleration at free-shaft to identify the magnetic model via adaptation in real-time. The proposed scheme systematically explores the  $dq$  current plane with a bipolar reference  $q$ -axis current  $i_q^*$  for torque reversals. The speed regulation is achieved by varying the duty-cycle of the bipolar  $i_q$  through a low-frequency pulse-width-modulation (LF-PWM) structure. Respect to [13], the proposed method characterizes the cross-saturation phenomenon with precision, although with the help of an encoder. The inability of [7] to characterize the self-saturation curves due to the zero torque areas is fixed in this new technique. Besides a position encoder, neither a dedicated rig nor any additional hardware is necessary. As many SyR machines are natively not provided with a position encoder, the proposed technique is also applicable as an end-of-line

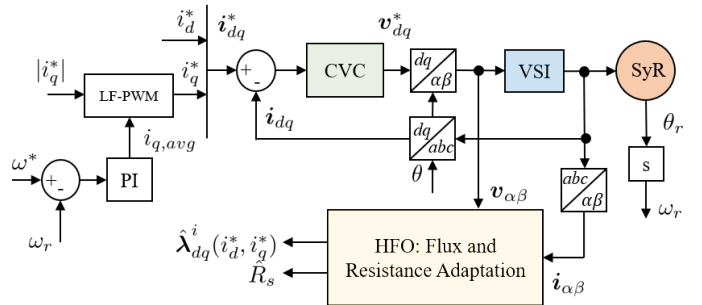


Fig. 1. Proposed MMI scheme: block diagram of current vector control (CVC) technique with low frequency pulse-width-modulation (LF-PWM) for  $q$ -axis current reference and online adaptation with hybrid flux observer (HFO).

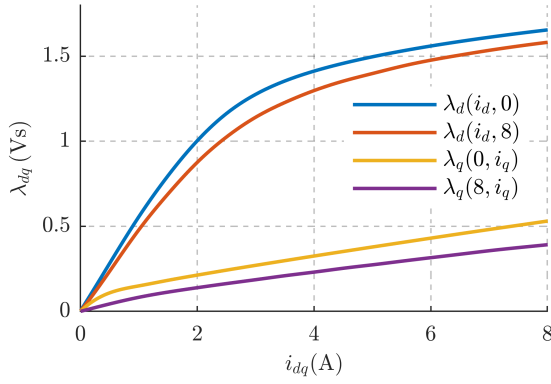


Fig. 2. Experimentally obtained flux-map of the 1.1 kW SyR motor under test with the constant speed test [4].

MMI, where the motor under test is coupled to an external encoder and identified within a few minutes, without the use of a prime mover or data recorders.

The projection vector framework is introduced in [15], [16] in the context of sensorless control where the discrepancy between the observed and the current-model flux estimates is used for position estimation. A similar framework is exploited for online stator flux and resistance adaptation.

The main features of this work are enumerated as follows:

- 1) Low-frequency modulated current references is proposed for speed regulation at free-shaft to systematically explore the  $dq$  current plane, as described in Section II.
- 2) The speed region of operation is optimized for a reliable flux estimation in the shortest time. The frequency of speed rate reversal is calibrated to limit the mechanical vibrations.
- 3) An online stator flux adaptation scheme is devised using the projection vector framework that makes the post-processing stage obsolete, as described in Section III.
- 4) Furthermore, a stator resistance adaptation is developed that tracks the temperature-induced variations and the non-ideal inverter dead-time compensation.
- 5) The adaptation laws are so formulated for the stator flux and the resistance to be decoupled and independent.

Experimental validation on a 1.1 kW SyR motor test bench is reported in the Section IV.

## II. PROPOSED CONTROL SCHEME FOR MMI

The electrical rotor position is  $\theta$  and the electrical angular speed is  $\omega = s\theta$  where  $s$  is the differential operator  $\frac{d}{dt}$ . Estimated vectors are represented by the superscript  $\hat{\cdot}$ . The orthogonal rotational matrix is  $\mathbf{J} = \begin{bmatrix} 0 & -1 \\ 1 & 0 \end{bmatrix}$  and  $\mathbf{I}$  is the identity matrix.

Real space vectors will be used; for example, the stator current is  $\mathbf{i}_{dq} = [i_d, i_q]^T$  where  $i_d$  and  $i_q$  are the vector components in rotor reference frame. Space vectors in the stationary reference frame are denoted by subscript  $\alpha\beta$ .

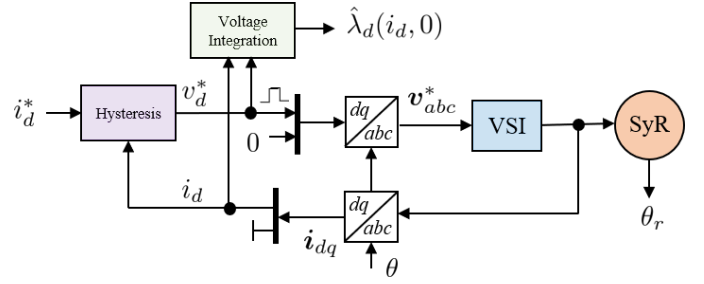


Fig. 3. Self-saturation identification test-d: Hysteresis current controller in  $d$ -axis with square-wave voltage injection and direct voltage integration.

### A. Synchronous Reluctance Machine Model

The voltage equation of a synchronous machine in rotor reference frame is expressed as

$$s \boldsymbol{\lambda}_{dq} = \mathbf{v}_{dq} - R_s \mathbf{i}_{dq} - \omega \mathbf{J} \boldsymbol{\lambda}_{dq} \quad (1)$$

where  $R_s$  is the stator resistance and  $\boldsymbol{\lambda}_{dq}$  is the stator flux linkage. All quantities are functions of  $\mathbf{i}_{dq}$ . The electromagnetic torque is given by

$$T = \frac{3p}{2} \mathbf{i}_{dq}^T \mathbf{J} \boldsymbol{\lambda}_{dq} \quad (2)$$

where  $p$  is the number of pole pairs.

The experimentally obtained flux-map of the SyR motor under test is shown in the Fig.2. The proposed magnetic model identification is comprised of two stages: i) test- $d$  and test- $q$  for self-saturation curves identification -  $\lambda_d(i_d, 0)$  and  $\lambda_q(0, i_q)$ , respectively; ii) test- $dq$  for cross-saturation curves identification.

### B. Self-Saturation Curves Identification at Standstill

In the first stage (test- $d$ ), the magnetic model of  $d$ -axis without cross-saturation ( $i_q = 0$ ) is identified with a hysteresis square-wave voltage injection as shown in the Fig.3, referred as test  $i$  in [13]. Similar exploration of  $q$ -axis (test- $q$ ) with hysteresis square-wave voltage injection at  $i_d = 0$  is referred as test  $ii$  in [13]. Respect to the sensorless implementation in [13], the presence of encoder permits extensive exploration of  $q$ -axis without problems of stability at high values of  $i_q$ .

The time-plots of the self-saturation identification test is shown in the Fig.4. Due to the smaller inductance along  $q$ -axis, a higher hysteresis frequency is observed. The square-wave voltage magnitude is set to 150 V (0.46 p.u.) and the current is limited to twice the rated value,  $i_d^* = i_q^* = 6.5$  A (2 p.u.). The stator flux is computed from the integration of voltage equation (1), shown in the Fig.5 where a good correlation with the reference curves is discerned. This initial self-saturation look-up tables (LUTs) are denoted as  $\hat{\boldsymbol{\Lambda}}_d$  and  $\hat{\boldsymbol{\Lambda}}_q$ .

### C. Cross-Saturation Identification

The control technique for cross-saturation identification at free-shaft, shown in Fig.1, is the integral contribution of this work. The self-saturation LUTs will be corrected for

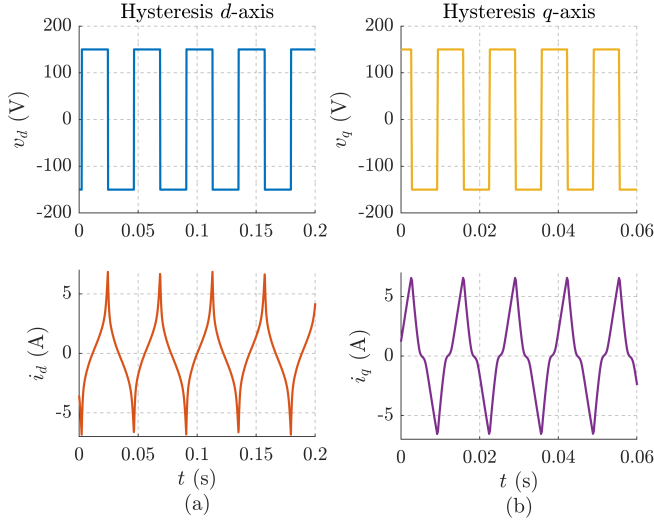


Fig. 4. Time plots of hysteresis controller for self-saturation identification: (a)  $d$ -axis excitation; (b)  $q$ -axis excitation.

including the cross-saturation current domain using an hybrid flux observer and a flux adaptation technique mutated from sensorless control, as described later. A closed-loop speed control is implemented with current vector control (CVC) scheme to impose reference current  $i_{dq}^*$ . The parameters from the self-saturation test can be used to tune the CVC regulators. A non-zero  $|i_d^*|$  and  $|i_q^*|$  couple generates electromagnetic torque and results in rotor movement. To limit the rotor speed, a bipolar reference for  $q$ -axis current is used for alternating acceleration and deceleration around the speed set-point, as shown in Fig. 6. The speed controller establishes an average speed equal to the reference speed by imposing an average  $q$ -axis current reference  $i_{q,avg}$ .

A low frequency pulse-width-modulation (LF-PWM) is used to calibrate the duty cycle of the bipolar  $i_q^*$  reference such that the mean value respects the speed controller commanded  $i_{q,avg}$ . The frequency of modulation  $f_q$  for LF-PWM should be an order higher than the bandwidth of speed controller.

Around nominal speed, iron losses gains significance whereas at very low speeds, flux estimation is unreliable due to the low signal-to-noise (SNR) of the back-emf signal integral. Hence, the mechanical speed span  $0.33 < |\omega_r| < 0.66$  p.u. is considered optimal for MMI, represented by the shaded region in Fig. 6(a). Ideally, it is desirable to confine the operation within optimal speed span by adapting the LF-PWM modulation frequency  $f_q$  as a function of the torque. However, this is not feasible due to the excessive mechanical vibrations for high  $f_q$  corresponding to high  $i_q^*$  and high torque. Alternatively, the maximum speed and the LF-PWM frequency  $f_q$  are held constant at 0.66 p.u (1000 rpm) and 15 Hz (experimentally calibrated), respectively while the lower speed limit (speed-span) varies according to the torque. To this end, the speed reference is determined as

$$\omega^* = (2\pi \cdot 25 \times 0.66) - \omega_{avg} \quad (3)$$

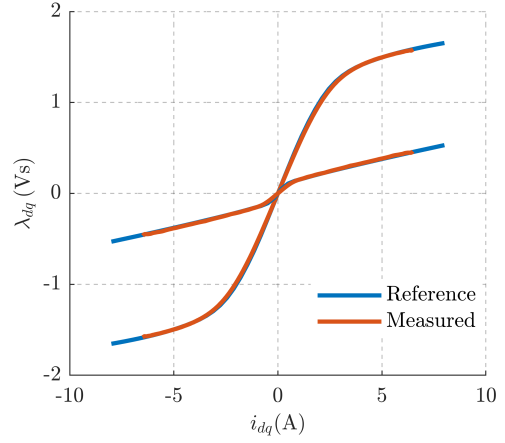


Fig. 5. Self-saturation identification curves from test- $d$  and test- $q$  with current limit  $i_d^* = i_q^* = 6.5$  A (2 p.u.) and superimposed over the reference curves, showing good correlation.

where  $\omega_{avg}$  is the mean of maximum and minimum speed in a LF-PWM cycle. It must be noted that only the data points within the optimal speed span are engaged in online flux and resistance adaptation, as discussed in the following.

### III. PROJECTION VECTOR FRAMEWORK FOR ONLINE ADAPTATION

The block diagram of proposed scheme with hybrid flux observer for online stator flux and resistance adaptation is shown in Fig. 7.

#### A. Hybrid Flux Observer

The state equation of the flux observer in stator reference frame is defined as

$$s\hat{\lambda}_{\alpha\beta} = \mathbf{v}_{\alpha\beta} - \hat{R}_s \mathbf{i}_{\alpha\beta} + \mathbf{G} (\hat{\lambda}_{\alpha\beta}^i - \hat{\lambda}_{\alpha\beta}) \quad (4)$$

where  $\mathbf{G} = g\mathbf{I}$  is a  $2 \times 2$  gain matrix,  $\hat{R}_s$  is the estimated stator resistance with error  $\tilde{R}_s = R_s - \hat{R}_s$  and  $\hat{\lambda}_{dq}^i$  is the LUTs-based current-model flux estimate with error  $\tilde{\lambda}_{dq}^i = \lambda_{dq}^i - \hat{\lambda}_{dq}^i$ . To aid in the analysis, the flux observer state equation (4) is transformed to the  $dq$  reference as

$$s\hat{\lambda}_{dq} = \mathbf{v}_{dq} - \hat{R}_s \mathbf{i}_{dq} - \omega \mathbf{J} \hat{\lambda}_{dq} + \mathbf{G} (\hat{\lambda}_{dq}^i - \hat{\lambda}_{dq}). \quad (5)$$

The term hybrid indicates that for the electrical speeds below  $g$  rad/s, the current-model flux linkage  $\hat{\lambda}_{dq}^i$  prevails while voltage-model flux linkage  $\lambda_{dq}$  for the speeds above.

#### B. Projection Vector Framework

The general error signal  $\epsilon$  is defined as the projection of the difference in observed and current-model flux estimates on a projection vector  $\phi$  [15], expressed as

$$\epsilon = \phi^T (\hat{\lambda}_{dq} - \hat{\lambda}_{dq}^i). \quad (6)$$

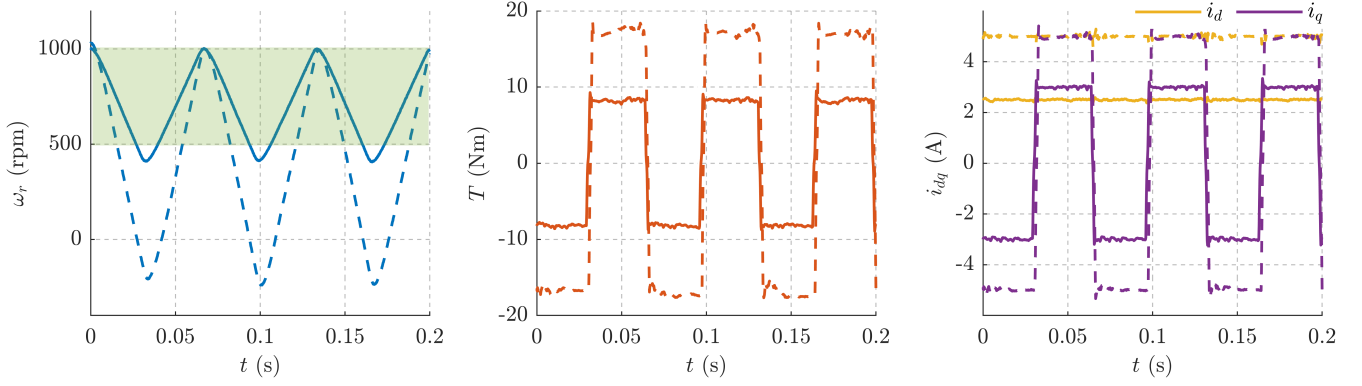


Fig. 6. Experimental time plots of cross-saturation identification: (a) Mechanical speed where the shaded region represents the optimal speed span for online adaptation; (b) Bipolar torque estimate; (c) Constant  $d$  and bipolar  $q$ -axis currents. Line Marker: continuous lines denote identification at  $i_d^* = 2.5$  &  $|i_q^*| = 3$  (A); dotted lines denote identification at  $i_d^* = 5$  &  $|i_q^*| = 5$  (A).

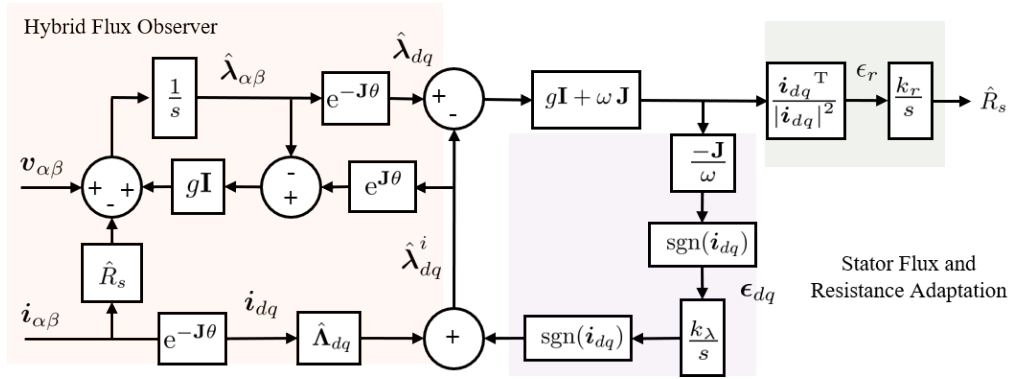


Fig. 7. Proposed scheme of hybrid flux observer with online current-model flux and stator resistance adaptation for cross-saturation identification.

It follows from (5) that the error signal  $\epsilon$  in terms of the current-model flux error  $\tilde{\lambda}_{dq}^i$  and the stator resistance error  $\tilde{R}_s$  is given by

$$\epsilon = \phi^T (s\mathbf{I} + \mathbf{G} + \omega\mathbf{J})^{-1} \cdot \left( (s\mathbf{I} + \omega\mathbf{J}) \tilde{\lambda}_{dq}^i + \tilde{R}_s \mathbf{i}_{dq} \right) \quad (7)$$

A similar error signal is used for rotor position estimation in sensorless control in [15], [16]. To aid in the design of projection vector in the following sections, the dc-component of the error signal (7) can be simplified as

$$\epsilon|_{s=0} = \phi^T (\mathbf{G} + \omega\mathbf{J})^{-1} \cdot \begin{bmatrix} -\omega \tilde{\lambda}_q^i + \tilde{R}_s i_d \\ +\omega \tilde{\lambda}_d^i + \tilde{R}_s i_q \end{bmatrix}. \quad (8)$$

Note that, due to the LF-PWM in  $q$ -axis, the terms  $i_q$  and  $\tilde{\lambda}_q^i$  in (8) are bipolar in nature. Moreover, the LUTs based current-model flux estimate consists here of the self-saturation curves only and it is therefore incomplete. The cross-saturation current domain part of the LUTs will be populated using the flux adaptation technique described in the following.

### C. Current-Model Flux Adaptation

Let  $\epsilon_d$  and  $\epsilon_q$  denote the LUTs-based current-model flux error signals along the projection vectors  $\phi_d$  and  $\phi_q$  for  $d$  and

$q$ -axis, respectively, expressed as

$$\epsilon_{dq} = \begin{bmatrix} \epsilon_d \\ \epsilon_q \end{bmatrix} = [\phi_d \ \phi_q]^T (\hat{\lambda}_{dq} - \hat{\lambda}_{dq}^i). \quad (9)$$

1) *d*-axis Adaptation: Using (8), the dc-component of the *d*-axis error signal is designed to be equal to the parameter error as

$$\epsilon_d|_{s=0} = \tilde{\lambda}_d^i \Rightarrow \phi_d^T = \frac{1}{\omega} [0 \ 1] (\mathbf{G} + \mathbf{J}\omega) \quad (10)$$

The *d*-axis flux adaptation is formulated to reflect the cross-saturation effect on the self-saturation stator flux from test-*d* as

$$\hat{\lambda}_d^i(i_d, i_q) = \hat{\Lambda}_d(i_d, 0) + \frac{k_\lambda}{s} \epsilon_d \quad (11)$$

where  $k_\lambda$  is the integral gain. The corresponding  $i_{dq}$  point of the  $\hat{\Lambda}_d$  LUTs is populated with the steady-state value of (11).

2) *q*-axis Adaptation: Despite the bipolar nature of the  $q$ -axis current, the error signal  $\epsilon_q$  is designed to be compatible with the adaptation law by transforming the parameter error to the first-quadrant (motoring) as

$$\begin{aligned} \epsilon_q|_{s=0} &= \tilde{\lambda}_q^i \cdot \text{sgn}(i_q) \\ \Rightarrow \phi_q^T &= \frac{-1}{\omega} [\text{sgn}(i_q) \ 0] (\mathbf{G} + \mathbf{J}\omega). \end{aligned} \quad (12)$$

Accounting for the polarity, the adaptation law supplements the cross-saturation offset to the self-saturation stator flux from test- $q$  as

$$\hat{\lambda}_q^i(i_d, i_q) = \hat{\Lambda}_q(0, i_q) + \text{sgn}(i_q) \cdot \frac{k_\lambda}{s} \epsilon_q. \quad (13)$$

As before, the  $\hat{i}_{dq}$  point of the  $\hat{\Lambda}_q$  LUTs is populated with the steady-state value of (13).

3) *Stator Resistance Sensitivity*: Under inaccurate resistance, the error signals  $\epsilon_d$  and  $\epsilon_q$  are accompanied by the resistance error term as

$$\epsilon_d|_{s=0} = \tilde{\lambda}_d^i + \frac{\tilde{R}_s}{\omega} i_q \quad (14a)$$

$$\epsilon_q|_{s=0} = \text{sgn}(i_q) \cdot \tilde{\lambda}_q^i - \frac{\tilde{R}_s}{\omega} \text{sgn}(i_q) \cdot i_d. \quad (14b)$$

It can be discerned that the resistance error bearing terms,  $i_q$  in (14a) and  $\text{sgn}(i_q) \cdot i_d$  in (14b), are bipolar in nature at the frequency  $f_q$ . At no load, the duty-cycle of LF-PWM is close to 0.5. Hence, the adaptation bandwidth is recommended to be less than one third of the LF-PWM frequency to filter out the bipolar signal, i.e.,  $k_\lambda < 0.33 \cdot 2\pi f_q$ . Thus, the flux adaptation turns out to be quasi-independent of resistance error.

#### D. Stator Resistance Adaptation

It is worth pointing out that, in addition to the two projection vectors (10) and (12), a third projection vector for stator resistance adaptation is feasible within the 2-D error domain ( $dq$ ) because of the bipolar nature of certain signals that are filterable.

Let  $\epsilon_r$  denote the resistance error signal. The resistance error projection vector  $\phi_r$  is designed using (8) such that the dc-component of the error signal is equal to the resistance error as

$$\epsilon_r|_{s=0} = \tilde{R}_s \Rightarrow \phi_r^T = \frac{\mathbf{i}_{dq}^T}{|\mathbf{i}_{dq}|^2} (\mathbf{G} + \mathbf{J}\omega). \quad (15)$$

Resistance adaptation law is expressed as

$$\hat{R}_s = \frac{k_r}{s} \epsilon_r \quad (16)$$

where  $k_r$  is the integral gain.

The influence of the current-model parameter errors on resistance adaptation is evaluated as

$$\epsilon_r|_{s=0} = \tilde{R}_s + \frac{\omega}{|\mathbf{i}_{dq}|^2} (\tilde{\lambda}_d^i i_q - \tilde{\lambda}_q^i i_d) \quad (17)$$

where the parameter error terms are bipolar in nature. As discussed before, a suitable selection of gain to filter out the bipolar signal is  $k_r < 0.33 \cdot 2\pi f_q$  and helps decoupling of the resistance adaptation from the current-model flux errors.

The fundamental component of the inverter voltage error due to non-ideal dead-time compensation is along the current vector [17]. The magnitude of the inverter voltage error is given by

$$\tilde{v}_{inv} = \frac{4}{3} v_{dc} f_s \tilde{t}_d \quad (18)$$

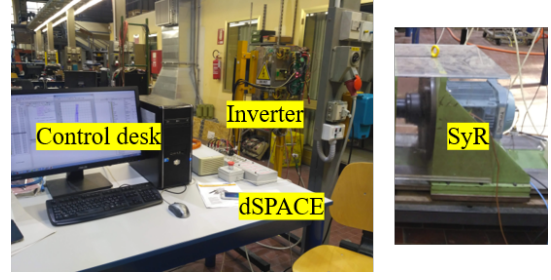


Fig. 8. Experimental Setup of 1.1 kW SyR motor under test on a dSPACE DS1103 control platform at a sampling frequency of 10 kHz.

TABLE I  
MOTOR AND INVERTER PARAMETERS

Parameters	Symbol	Values	Units
Rated power	$P_n$	1.1	kW
Rated voltage	$V_n$	340	V
Rated speed	$\omega_n$	1500	rpm
Rated current	$I_n$	2.3	A
Rated torque	$T_n$	7.1	Nm
Pole pairs	$p$	2	-
Stator resistance	$R_s$	5.9	$\Omega$
Motor inertia	$J$	0.004	kgm <sup>2</sup>
Nominal dead-time	$t_d$	1.9	$\mu\text{s}$
DC-link voltage	$v_{dc}$	565	V

where  $\tilde{t}_d$  is the error in compensated dead-time,  $f_s$  is the inverter PWM frequency and  $v_{dc}$  is the DC-link voltage. Hence, the effective estimated resistance is given by

$$\hat{R}_s = R_s + \frac{1}{|\mathbf{i}_{dq}|} \cdot \frac{4}{3} v_{dc} f_s \tilde{t}_d. \quad (19)$$

#### IV. EXPERIMENTAL RESULTS

The proposed scheme is validated experimentally on a 1.1 kW SyR motor on a dSPACE DS1103 control platform running at a sampling frequency of 10 kHz. A picture of the setup is shown in Fig. 8. The parameters of the SyR motor under test are tabulated in Table I.

The speed controller bandwidth is set to  $2\pi \cdot 1$  rad/s. The flux observer gain is  $g = 2\pi \cdot 10$  rad/s. The adaptation gains are  $k_\lambda = 2\pi \cdot 2.5$  rad/s and  $k_r = 2\pi \cdot 0.5$  rad/s.

##### A. Dynamics of Current-Model Flux Adaptation

The time-plots of the current-model adaptation is shown in the Fig.9 for the set-points  $i_d^* = 5$  A (1.5 p.u.) and  $i_q^* = 5$  A (1.5 p.u.). The speed-swing for these reference points is observed to be approximately 1000 rpm although the adaptation, if enabled, is only active for speeds greater than 500 rpm,  $\omega_r > 500$  rpm.

The adaptation is enabled at  $t = 0$  s. For  $t < 0$  s, the current-model flux estimates are derived from the self-saturation identification and hence, an error of  $\tilde{\lambda}_d^i = 0.04$  Vs and  $\tilde{\lambda}_q^i = 0.07$  Vs exists due to the cross-saturation effect. Once the adaptation is enabled at  $t > 0$  s, the errors reduce to  $\tilde{\lambda}_d^i = 0.015$  Vs (0.014 p.u.) and  $\tilde{\lambda}_q^i = 0.002$  Vs (0.002 p.u.). The settling time is observed to be around 0.75 s. A



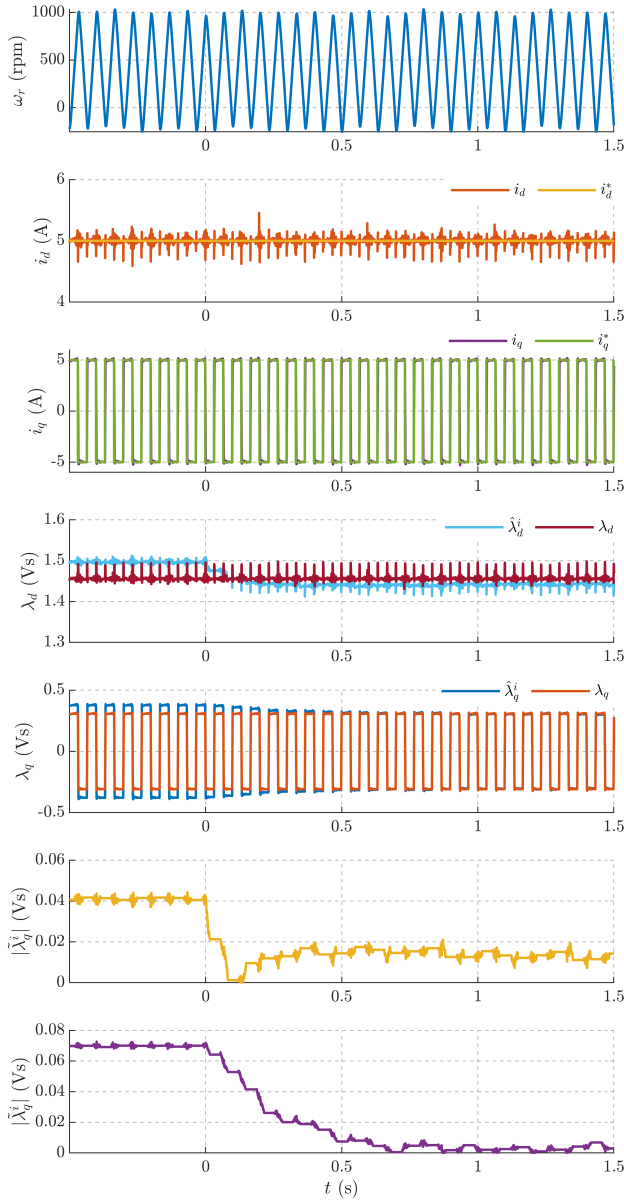


Fig. 9. Time plots to illustrate the dynamics of current-model flux adaptation at  $i_d^* = 5$  A (1.5 p.u.) and  $i_q^* = 5$  A (1.5 p.u.). The adaptation is enabled at  $t = 0$  s.

small error in the  $d$ -axis remains which is likely due to the iron losses at high speed.

### B. Systematic MMI with Current-Model Flux Adaptation

The  $dq$  current plant is systematically explored for the cross-saturation identification. A minimum torque is necessary for speed regulation; as the motor under test is in free-shaft condition and disconnected from load, a minimum of  $i_{d,min}^* = |i_{q,min}^*| = 0.5$  A (0.15 p.u.) on either axes is found sufficient for speed regulation. The maximum current is determined the inverter limits, subject to the voltage constraint at the maximum speed (1000 rpm); a 50% overload in either

axes is found achievable, i.e.,  $i_{d,max}^* = |i_{q,max}^*| = 5$  A (1.5 p.u.).

The control systematically traverses the  $dq$  current plane from  $i_{dq,min}^*$  to  $i_{dq,max}^*$  in steps of 0.5 A, resulting in a  $10 \times 10$  grid with 100 data-points. For each set of the references, a small time is elapsed ( $\approx 2$  s) to allow the dynamics of the adaptation to settle down to a steady-state before data acquisition. The total elapsed time per data-point is about 3.5 s and for the complete cross-saturation identification test is around six minutes.

As formerly discussed, the online adaptation is enabled only in the optimal speed-span for speeds greater than 500 rpm. The Fig. 10(a) juxtaposes the identified flux curves against the reference curves that shows good correlation. The current-model flux error contours of  $d$  and  $q$ -axis are shown in the Fig. 10(b) and 10(c), respectively. The error increases at high load with the maximum of around 0.015 Vs. The  $q$ -axis estimate is inaccurate near the origin due to the sharp saturation of ribs.

### C. Stator Resistance Adaptation

The stator resistance adaption is concurrently active along with the stator flux adaptation in the previous section. The Fig. 11(a) shows the contour plot of the effective estimated resistance that inherently accounts for non-idealities in the dead-time compensation as per (19). For a better understanding, the net voltage accounting the resistance drop and the dead-time non-ideal compensation is computed in the contour plot Fig. 11(b) where a function of the stator current magnitude emerges.

The characterization of the stator resistance and the dead-time error is carried out in the Fig. 11(c) from which the stator resistance is evaluated to  $R_s = 5.9 \Omega$  and the dead-time error to  $\tilde{t}_d = -0.3 \mu\text{s}$ . Thus, besides estimation of stator resistance, the proposed adaptation also helps to mitigate the non-idealities in the inverter dead-time compensation.

## V. CONCLUSION

A self-commissioning technique for magnetic-model-identification for SyR machines at free-shaft is proposed. The self-saturation flux curves are obtained from the common hysteresis current controller with square-wave voltage injection. A novel LF-PWM scheme for speed regulation via bipolar  $i_q$  is developed for cross-saturation identification. The maximum speed is held constant at 0.66 p.u. to limit the iron losses while the lower limit of the speed-swing varies according to the torque produced at each operating point.

The cross-saturation domain of the flux-map LUTs is built using a projection-vector based stator flux adaptation scheme. Moreover, an additional projection vector is used to compensate for the stator resistance and inverter dead time voltage errors. The adaptation laws are formulated such that the stator flux and the resistance are independent and decoupled.

The proposed scheme is experimentally validated on a 1.1 kW SyR motor test-bench. The identified flux-map shows good correlation with the reference maps and the maximum

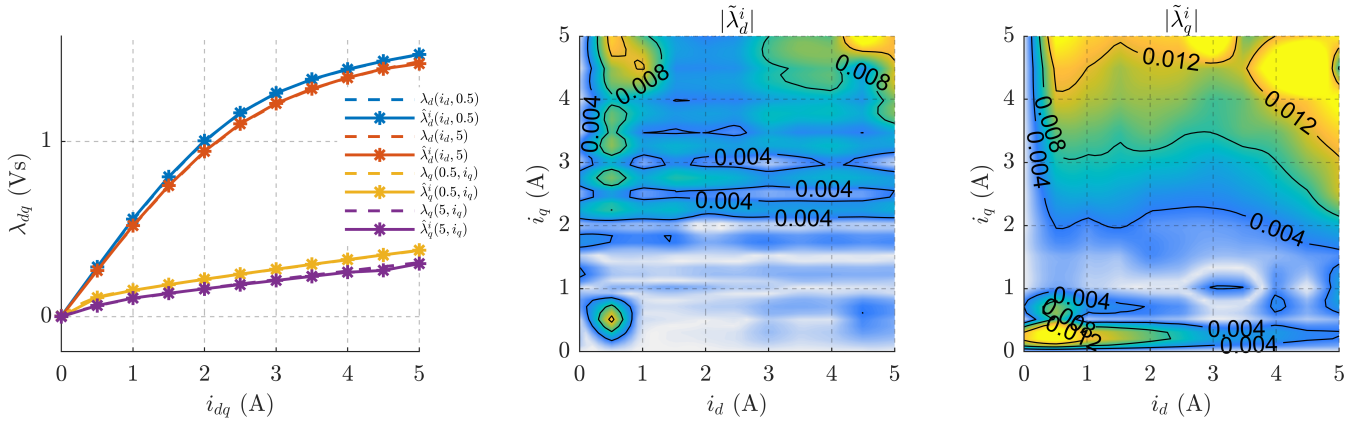


Fig. 10. Experimental MMI with self and cross-saturation: (a) Identified curves shown against reference flux-map, showing good correlation; (b) Error contour in  $d$ -axis in Vs; (c) Error contour in  $q$ -axis in Vs.

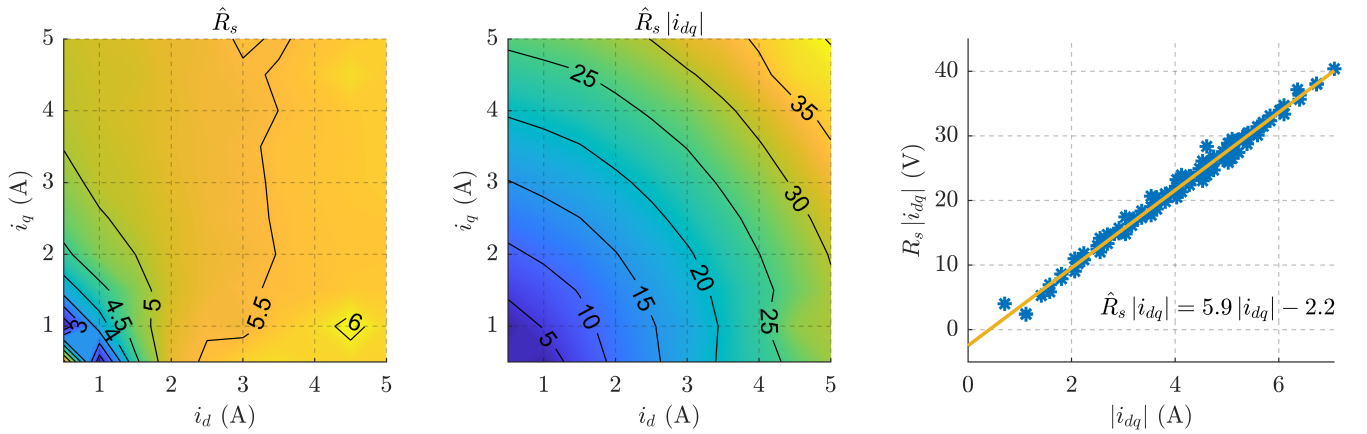


Fig. 11. Stator resistance adaptation in the experimental MMI: (a) Effective estimate resistance accounting the dead-time inaccuracy (19); (b) Net voltage accounting the resistance drop and the dead-time non-ideal compensation; (c) Characterization of the stator resistance and the inverter dead-time (fundamental component).

error is around 0.015 Vs (0.014 p.u.) at high loads, producing negligible error in the interpretation of optimal operation with MTPA and MTPV laws.

## REFERENCES

- [1] H. A. A. Awan, Z. Song, S. E. Saarakkala, and M. Hinkkanen, "Optimal Torque Control of Saturated Synchronous Motors: Plug-and-Play Method," *IEEE Transactions on Industry Applications*, p. 1, 2018.
- [2] G. Pellegrino, R. I. Bojoi, and P. Guglielmi, "Unified direct-flux vector control for AC motor drives," *IEEE Transactions on Industry Applications*, vol. 47, no. 5, pp. 2093–2102, 2011.
- [3] IEEE, "IEEE Trial-Use Guide for Testing Permanent Magnet Machines," pp. 1–56, 2015.
- [4] E. Armando, R. I. Bojoi, P. Guglielmi, G. Pellegrino, and M. Pastorelli, "Experimental identification of the magnetic model of synchronous machines," *IEEE Transactions on Industry Applications*, vol. 49, no. 5, pp. 2116–2125, 2013.
- [5] S. A. Odhano, R. Bojoi, t. G. Roşu, and A. Tenconi, "Identification of the Magnetic Model of Permanent-Magnet Synchronous Machines Using DC-Biased Low-Frequency AC Signal Injection," *IEEE Transactions on Industry Applications*, vol. 51, no. 4, pp. 3208–3215, 2015.
- [6] L. Peretti, P. Sandulescu, and G. Zanuso, "Self-commissioning of flux linkage curves of synchronous reluctance machines in quasi-standstill condition," *IET Electric Power Applications*, vol. 9, no. 9, pp. 642–651, 2015.
- [7] G. Pellegrino, B. Boazzo, and T. M. Jahns, "Magnetic Model Self-Identification for PM Synchronous Machine Drives," *IEEE Transactions on Industry Applications*, vol. 51, no. 3, pp. 2246–2254, 2015.
- [8] K. Liu, J. Feng, S. Guo, L. Xiao, and Z. Zhu, "Identification of Flux Linkage Map of Permanent Magnet Synchronous Machines Under Uncertain Circuit Resistance and Inverter Nonlinearity," *IEEE Transactions on Industrial Informatics*, vol. 14, no. 2, pp. 556–568, 2018.
- [9] N. Bedetti, S. Calligaro, and R. Petrella, "Stand-Still Self-Identification of Flux Characteristics for Synchronous Reluctance Machines Using Novel Saturation Approximating Function and Multiple Linear Regression," *IEEE Transactions on Industry Applications*, vol. 52, no. 4, pp. 3083–3092, 2016.
- [10] S. Wiedemann and R. M. Kennel, "Encoderless self-commissioning and identification of synchronous reluctance machines at standstill," in *IEEE International Symposium on Industrial Electronics*, 2017, pp. 296–302.
- [11] M. Hinkkanen, P. Pescetto, E. Mölsä, S. E. Saarakkala, G. Pellegrino, and R. Bojoi, "Sensorless Self-Commissioning of Synchronous Reluctance Motors at Standstill Without Rotor Locking," *IEEE Transactions on Industry Applications*, vol. 53, no. 3, pp. 2120–2129, 2017.
- [12] P. Pescetto and G. Pellegrino, "Automatic Tuning for Sensorless Commissioning of Synchronous Reluctance Machines Augmented with High-Frequency Voltage Injection," *IEEE Transactions on Industry Applications*, vol. 54, no. 5, pp. 4485–4493, 2018.
- [13] A. Varatharajan, P. Pescetto, and G. Pellegrino, "Sensorless Self-Commissioning of Synchronous Reluctance Machine with Rotor Self-Locking Mechanism," in *2019 IEEE Energy Conversion Congress and Exposition (ECCE)*, 2019, pp. 812–817.



- [14] S. A. Odhano, P. Pescetto, H. A. A. Awan, M. Hinkkanen, G. Pellegrino, and R. Bojoi, "Parameter Identification and Self-Commissioning in AC Motor Drives: A Technology Status Review," *IEEE Transactions on Power Electronics*, vol. 34, no. 4, pp. 3603–3614, 2019.
- [15] M. Hinkkanen, S. E. Saarakkala, H. A. A. Awan, E. Mölsä, and T. Tuovinen, "Observers for Sensorless Synchronous Motor Drives: Framework for Design and Analysis," *IEEE Transactions on Industry Applications*, vol. 54, no. 6, pp. 6090–6100, 2018.
- [16] A. Varatharajan and G. Pellegrino, "Sensorless Synchronous Reluctance Motor Drives: A General Adaptive Projection Vector Approach for Position Estimation," *IEEE Transactions on Industry Applications*, vol. 56, no. 2, pp. 1495–1504, 2020.
- [17] G. Pellegrino, P. Guglielmi, E. Armando, and R. I. Bojoi, "Self-commissioning algorithm for inverter nonlinearity compensation in sensorless induction motor drives," *IEEE Transactions on Industry Applications*, vol. 46, no. 4, pp. 1416–1424, 2010.